# Weakening of western disturbances in response to polar sea ice melt in climate model simulations

**Varunesh Chandra**
Indian Institute of Technology Delhi
**Sukumaran Sandeep** (sandeep.sukumaran@cas.iitd.ac.in)
Indian Institute of Technology Delhi
**Kieran M R Hunt**
University of Reading

---

**Research Article**

**Keywords:** Polar Sea Ice, Western Disturbance (WDs), Westerly Jet

**Posted Date:** October 10th, 2022

**DOI:** https://doi.org/10.21203/rs.3.rs-2132087/v1



---

# Weakening of western disturbances in response to polar sea ice melt in climate model simulations

**Varunesh Chandra · S. Sandeep · Kieran M. R. Hunt**

Received: date / Accepted: date

**Abstract** The response of low-latitude weather and climate to polar sea ice melt is not well understood. In this study, we run a suite of coupled and uncoupled simulations using the Community Earth System Model to investigate the effects of polar sea ice melt on western disturbance (WD) activity over the Indian subcontinent. In the coupled model simulation, the albedo of the sea ice is reduced in such a way that the increased absorption of the solar radiation would melt the sea ice. Further, the monthly climatology of sea surface temperature (SST) and sea ice concentrations (SIC) from the coupled model runs are used to force the Community Atmospheric Model (CAM5) at higher resolution (50 km). WD vortices in the CAM5 simulations are tracked using a Lagrangian tracking algorithm. Our analyses reveal that WD activity is reduced in the CAM5 simulations forced with the SST and SIC from the sea ice melt experiment. We show that this is because the subtropical jet becomes more baroclinically stable and shifts equatorward in response to the polar sea ice melt. The weakening and widening of the subtropical jet is consistent with the predicted changes to thermal wind and upper-tropospheric meridional temperature gradient in response to the polar sea ice melt.

**Keywords** Polar Sea Ice · Western Disturbance (WDs) · Westerly Jet

## 1 Introduction

One of the major concerns of the global warming is its effect on polar sea ice. Sea ice melt can have far reaching and long lasting implications on the climate system. Observations show that the Arctic sea ice extent (SIE) has been declining since 1970s, with the summer SIE reduced by half (NSIDC, 2022); however, Antarctic

Varunesh Chandra and S. Sandeep
Centre for Atmospheric Sciences, Indian Institute of Technology Delhi, New Delhi 110016, India
E-mail: sandeep.sukumaran@cas.iitd.ac.in
Kieran M. R. Hunt
Department of Meteorology, University of Reading, Reading, UK

sea ice has demonstrated complex variability over the same period. The southern hemispheric SIE increased at a rate of 2% per decade during 1979–2015 followed by a rapid decline in the last few years (Comiso et al., 2017; NSIDC, 2022). Climate model projections using high emission scenarios indicate that both the Arctic and Antarctic will start experiencing ice free summers by the middle and late 21$^{st}$ century respectively (Collins et al., 2013; Liu et al., 2013; Overland and Wang, 2013; Jahn et al., 2016). Sea ice melt has far reaching effects on the global climate system through surface energy imbalance and the subsequent response of ocean dynamics (Screen and Simmonds, 2010; Serreze and Barry, 2011). Further, the thermal inertia of the oceans cause the effects of sea ice melt to persist for several decades. Experiments using uncoupled general circulation models have shown that depletion of Arctic sea ice explains most of the seasonal pattern of the high-latitude climate response to greenhouse gas-induced warming (Deser et al., 2010).

Melting of sea ice results in a reduction of surface albedo and as result, enhanced absorption of shortwave radiation at the surface. This process leads to a positive feedback loop that amplifies the sea ice melt. Over the Arctic, this feedback has resulted in a rapid warming of the surface temperature, known as Arctic Amplification (Serreze and Francis, 2006; Holland and Bitz, 2003; Dai, 2021). One of the consequences of the rapid surface warming of the Arctic compared to the rest of the globe is that it weakens the equator to pole temperature gradient. Evidence already indicates that the meridional temperature gradient in the lower troposphere over the northern hemisphere is weakening (Francis and Vavrus, 2012; Haarsma et al., 2013; Francis and Vavrus, 2015). This pattern is reversed in the upper troposphere, where the tropics warm faster than the poles, resulting in a strengthening of the meridional temperature gradient Thompson and Solomon (2005); Allen and Sherwood (2008); Harvey et al. (2014). These contrasting changes have resulted in increased vertical shear in extratropical jets (Lee et al., 2019).

The response of subtropical and low latitude circulations to the polar sea ice melt is not well understood. Unlike the extratropical jet that is mostly driven by the thermal wind balance, the subtropical jet (STJ) is a response to both thermal wind balance and angular momentum conservation (Krishnamurti, 1961; Held and Hou, 1980). During boreal summer, the STJ weakens and moves poleward of 35°N, while in winter it intensifies and shifts equatorward, often passing over the Western Himalaya. The observations suggest that the STJ has become more wavy in the recent decades in response to an overall weakening of the meridional temperature gradient (Francis and Vavrus, 2015).

Baroclinic instability associated with the STJ creates favourable conditions for the growth of synoptic-scale baroclinic disturbances known as western disturbances (WDs; Dimri et al., 2016; Hunt et al., 2018a; Hunt and Zaz, 2022). WDs play an important role in the production of winter and spring precipitation over the northwestern part of the Indian subcontinent and the Himalayas (Mooley, 1957; Rangachary and Bandyopadhyay, 1987; Houze et al., 2011; Dimri et al., 2015; Houze et al., 2017; Hunt et al., 2018a). They are therefore crucial for water security over the Himalayan region (Dimri, 2013; Iqbal and Ilyas, 2013). WDs can also cause hazards over South Asia. For example, a large majority of recent landslides over the western Himalayas and Karakoram have been triggered by heavy precipitation brought by WDs (Hunt and Dimri, 2021). WDs have also been linked to catastrophic floods, such as those that occurred over Uttarakhand in 2013 (Chevuturi and Dimri, 2016; Hunt et al., 2021).

The interannual variability of WDs is driven in part by teleconnections with the tropical Pacific and Atlantic, with the El Niño Southern Oscillation (ENSO) and the North Atlantic Oscillation (NAO) playing key roles (Yadav et al., 2009; Dimri, 2013; Filippi et al., 2014). The relative strengths of these teleconnections has varied over the last century, with Yadav et al. (2009) noting an increasing influence of ENSO and decreasing influence of the NAO on winter precipitation over northwestern India since 1950. The STJ acts as a medium for these remote climate forcings to influence WD activity (Hunt and Zaz, 2022). In this context, we may anticipate that the response of STJ to the polar sea ice melting can influence the formation and intensification of WDs, subject to the caveat that the strength of this relationship may not be constant in time.

Few studies have explored how WDs respond to projected future warming in climate models and those that have disagree on the sign of change depending on the methodology used. Studies that use proxies for WD activity (e.g., filtered 500 hPa geopotential variance) have found a weak positive trend over the coming century (Ridley et al., 2013; Krishnan et al., 2018). However, results from applying a WD-tracking algorithm to the CMIP5 multimodel ensemble showed a robust weakening trend, with a drop of 15% in the frequency and 12% in the intensity of the storms by the end of $21^{\mathrm{st}}$ century (Hunt et al., 2019a). They attributed the decline in the WD activity to the weakening of STJ in a warming climate. The polar sea ice melt can also elicit a climate system response similar to that of global warming (England et al., 2020). Recent studies using coupled models suggest that both Arctic and Antarctic sea ice melt can influence changes in the deep tropics (Liu and Fedorov, 2019; England et al., 2020; Chandra et al., 2022). Using climate model simulations, Chandra et al. (2022) showed that the Indian summer monsoon circulation and synoptic activity would weaken in response to the polar sea ice melt. Here, we use the modeling framework from Chandra et al. (2022) to investigate the changes in WD activity in response to the polar sea ice melt.

## 2 Data and methods

### 2.1 Coupled and uncoupled climate model simulations

The presence of multiple modes of spatiotemporal variability, as well as various feedback effects, pose a challenge in extracting the effect of sea ice melt on climate system. A robust way to isolate the effect of sea ice melt on the rest of the climate system is by forcing the sea ice to melt in a coupled climate model by either lowering the albedo of the sea ice or adding additional heat to the polar region (Screen et al., 2018). The addition of extra heat would result in a violation of conservation of energy, and hence we choose the albedo reduction method. A contrast between a benchmark simulation and the run in which the sea ice is forced to melt can quantify the effect of the sea ice melt on climate and long-term weather variability. We used the community earth system model (CESM) version 1.1.2 (Hurrell et al., 2013) to perform idealized experiments. We chose a horizontal resolution of $0.9^{\circ}\times1.25^{\circ}$ for land and atmosphere, while the ocean and sea ice components share a variable resolution displaced pole grid (gx1v6). The atmospheric component of the model has 32 hybrid sigma-pressure vertical levels.

Firstly, the CESM model is run in a fully coupled configuration for 350 years with pre-industrial forcing (B1850). We call this the control experiment (CTRL). In the second experiment, the model was restarted from the 300$^{\text{th}}$ year of CTRL and run for an additional 50 years. In this latter experiment, the albedo of bare and ponded sea ice, as well as snow cover on ice, over the Arctic and Antarctic Oceans in the sea ice component was reduced. Specifically, we changed the values of two non-dimensional tuning parameters $R_{ice}$ and $R_{pnd}$, in the solar radiation parameterization scheme of the sea ice component, from 0 to -2. This change would result in a reduction of sea ice albedo by about 6.3% (Briegleb and Light, 2007). In addition, for all spectral bands, we reduced the single scattering albedo of snow by 10%. These changes are made following Liu and Fedorov (2019), who found that the chosen values closely replicated recent sea ice loss. We refer to this experiment as the sea ice melt experiment (SIME).

Transient weather systems, such as WDs, may not be adequately resolved in these coarse resolution simulations (Hunt et al., 2019b). Hence, we also designed an ensemble of high-resolution Community Atmospheric Model (CAM5) simulations that use the sea surface temperature (SST) and sea ice concentration (SIC) annual cycles from the coupled model simulations. The last ten years of CTRL and SIME simulations were used to construct the annual cycles of the monthly climatology of SST and SIC. To distinguish the CAM5 experiments from the fully coupled CESM experiments, we call them CTRL-CAM5 and SIME-CAM5, respectively. For both experiments, the remaining CAM5 forcings are set to year 2000 conditions. For both CAM5-CTRL and CAM5-SIME, we ran an ensemble of four runs each, by slightly perturbing the initial surface temperature. Each of these runs span for four years, giving a total of sixteen years of data. Similar high-resolution atmospheric model simulations have been performed to investigate the changes in monsoon low-pressure systems (Sandeep et al., 2018; Chandra et al., 2022).

### 2.2 Tracking of western disturbances

We used the Lagrangian tracking algorithm described in Hunt et al. (2018b, 2019c) to track WDs in the high-resolution CAM5 simulations. When applied to six-hourly reanalysis or climate model data, as in Hunt et al. (2018b, 2019c), the algorithm identifies local maxima in T63 spectrally-truncated instantaneous 450-300 hPa relative vorticity, subject to an 850 km search radius. These maxima are linked across timesteps through a biased nearest-neighbour search, with system propagation speed limited to 1000 km (6 hr)$^{-1}$. A final round of filtering ensures that (a) tracks last at least 48 hours; (b) tracks pass through [20-36.5°N, 60-80°E]; and (c) track endpoints are to the east of their geneses. To account for the CAM5 simulations having only daily output and lower vertical resolution than the reanalysis used in Hunt et al. (2019c), we have made three small adjustments to the algorithm sensitivity. Firstly, we use 500-200 hPa relative vorticity; secondly, we impose a minimum track duration of three days; thirdly we impose a maximum propagation speed of 2500 km day$^{-1}$.

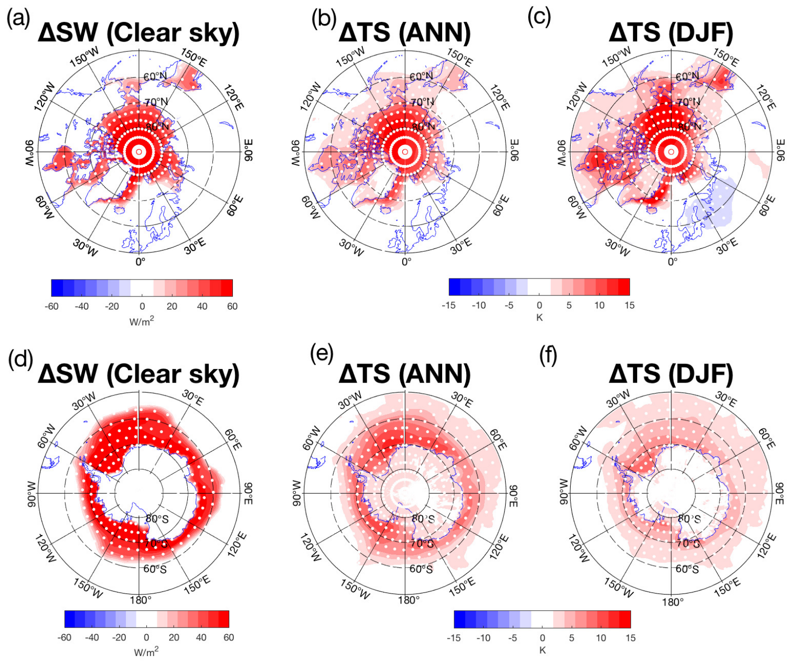


**Fig. 1** The difference between SIME and CTRL over the Arctic in (a) the annual mean climatology of clear sky net solar flux at surface, (b) the annual mean climatology of surface temperature, and (c) the DJF mean climatology of surface temperature. (d) - (f) Same as (a) - (c), except for the Antarctic. The climatology is constructed using the last 10 years of CTRL and SIME runs.

## 3 Results and discussion

The imposed reduction of snow and ice albedo in the model should result in an enhanced absorption of the shortwave radiation at the surface. The annual mean difference in the clear sky shortwave radiation between the SIME and CTRL experiments shows an additional shortwave radiation of about 60 W m$^{-2}$ over the northern hemispheric sea ice regions (Fig. 1a). This additional shortwave radiation at surface in the SIME simulation resulted in an annual mean surface warming of about 15 K compared to the CTRL experiment (Fig. 1b). The December–January (DJF) mean surface temperature difference between the SIME and CTRL shows a stronger warming of about 20 K (Fig. 1c). The highest warming occurred over the Arctic circle and the pattern weakened towards the equator. This suggests a weakening of the lower-tropospheric equator to pole temperature gradient. In the southern hemisphere, the magnitude of additional surface shortwave radiation in the SIME simulation is similar to that of northern hemisphere (Fig. 1d). However, both the annual and DJF mean surface warming are weaker compared to the corresponding patterns over the northern hemisphere (Figs. 1e, f).

The ensemble mean DJF track density of WDs in the CTRL-CAM5 shows a peak over the northwestern India and Pakistan (Fig. 2a). The spatial distribution

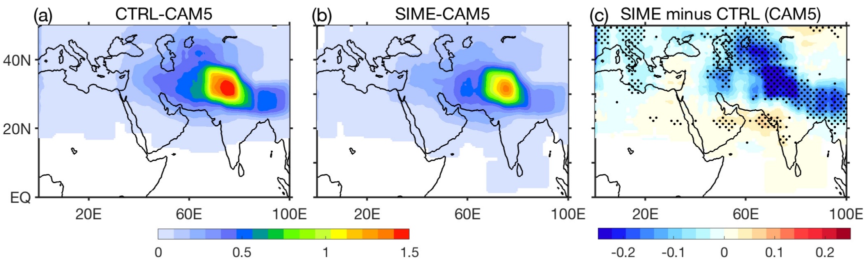


**Fig. 2** DJF mean, ensemble mean WD track density (unit: number of LPS per grid per season) for (a) CTRL-CAM5 and (b) SIME-CAM5 simulations, and (c) ensemble mean SIME-CAM5 minus CTRL-CAM5 track density. Stippling in (c) denote the statistically significant (at 95% confidence level) difference between SIME-CAM5 and CTRL-CAM5 track density, as revealed by a bootstrapping method

of WD activity in CTRL-CAM5 simulations is consistent with that seen in the observations and CMIP5 historical simulations (Hunt et al., 2018b, 2019c). The pattern of WD track density in the SIME-CAM5 ensemble also has a similar spatial structure, but with a clear and statistically signficant weakening of the magnitude (Fig. 2b). In fact, the ensemble mean difference between SIME-CAM5 and CTRL-CAM5 shows about 19% weakening in WD track density over the core region of WD activity, in response to the polar sea ice melting. The weakening of WDs in SIME-CAM5 simulations is similar to that seen in the simulations under strong warming scenario (Hunt et al., 2019a). This suggests that, in climate model simulations, the response of WDs to the polar sea ice melting is similar to its changes due to external radiative forcing. This is in line with the similarities in the larger climate system responses to the imposed sea ice melt and greenhouse gas induced warming (England et al., 2020).

It is also necessary to examine if the intensity of WDs also undergo a change as in the case of their frequency, since precipitation scales with WD intensity and hazardous precipitation is associated with the strongest WDs (Hunt et al., 2018b,c). Here, we follow convention and use mid-tropospheric (500 hPa) absolute vorticity as an indicator of WD strength. The storm-centered composite of ensemble mean absolute vorticity for the WDs simulated by CTRL-CAM5 simulations show a well defined pattern with maximum values lying close to the center of the storms (Fig. 3a). The same calculations for the WDs in SIME-CAM5 simulations also show a coherent spatial structure of mid-tropospheric vorticity associated with the WDs, but with substantial weakening in the values (Fig. 3b). The difference plot between SIME-CAM5 and CTRL-CAM5 shows that the mean absolute vorticity associated with the WDs weakened substantially and significantly in response to the polar sea ice melt (Fig. 3c). The time average field does not reveal any shifts in the WD intensity towards stronger or weaker vorticity during the lifecycle of the storm. For example, a higher number of weaker storm days at the expense of stronger ones, cannot be revealed by the vorticity averaged over the lifecycle of WDs. To examine the possibility of any such shifts in the frequency of storm days towards the weaker or stronger side, we constructed the distribution of the number of WD days as a function of daily maximum relative vorticity (Fig. 3d). This analysis reveals that the weakening of WDs happen across all intensity

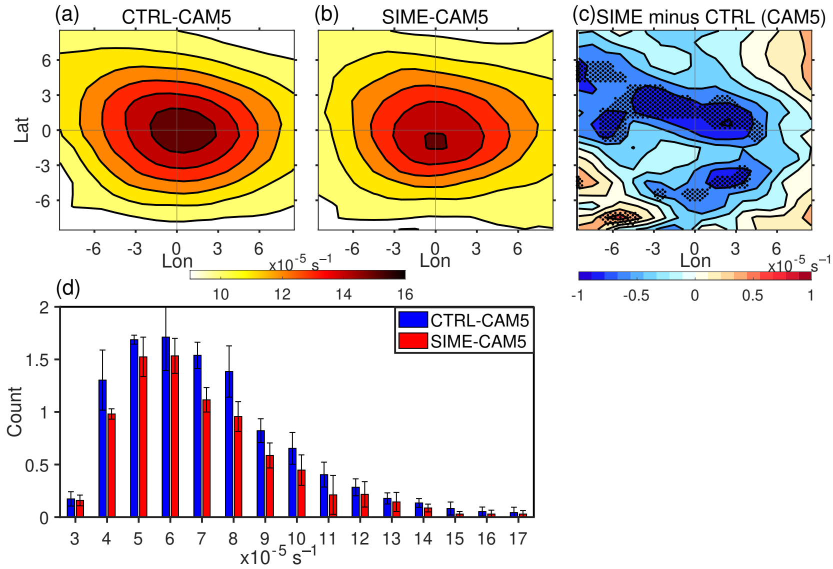


**Fig. 3** DJF mean, ensemble mean of system-centered composite structure of 500-hPa absolute vortices for (a) CTRL-CAM5 and (b) SIME-CAM5 simulations, and (c) ensemble mean SIME-CAM5 minus CTRL-CAM5 absolute vortices; (d) distribution of daily maximum relative vorticity during WD life cycle, from CTRL-CAM5 and SIME-CAM5 simulations. Stippling in (c) denote the statistically significant (at 95% confidence level) difference between SIME-CAM5 and CTRL-CAM5 absolute vortices, as revealed by a bootstrapping method. The error bars in (d) show ensemble spread ($\pm 1\sigma$) of CTRL-CAM5 and SIME-CAM5 runs.

bands, and there is no shift towards high or low intensity storm days, in a polar sea ice melt scenario. Thus, both frequency and intensity of WDs decrease in SIME-CAM5 simulations, indicating that the climate system response to the polar sea ice melt might have affected the large-scale processes that control the WD genesis and development. The decline in the intensity of the WDs in SIME-CAM5 ensemble is consistent with the weakening of the WD intensity reported by Hunt et al. (2019a) in their analysis of WD activity by the end of the 21$^{st}$ century under future warming projections.

The baroclinic instability associated with the subtropical jetstream (STJ) creates a favourable condition for the genesis and development of WDs (Dimri, 2013; Hunt et al., 2018b; Hunt and Zaz, 2022). The interannual variability in WD activity and winter precipitation over the western Himalayan and Hindu Kush region have been linked to the variability in the STJ (Yadav et al., 2009; Filippi et al., 2014; Hunt and Zaz, 2022). Therefore, the response of STJ to the polar sea ice melt needs to be carefully examined. Hunt et al. (2018b) identified that both the latitudinal location and intensity of the jet control the WD activity. We compare the distributions of WD counts and the frequency of persistence of STJ as a function of latitude in the CAM5 simulations (Fig. 4a, b). We define the STJ core as the maximum of monthly mean zonal mean (60°E–85°E) zonal winds at 200 hPa during December, January, and February. A comparison between the two shows that WD latitudes have a similar distribution to that of the background STJ. WDs exhibit slightly greater variance here because the distributions comprise individual WDs

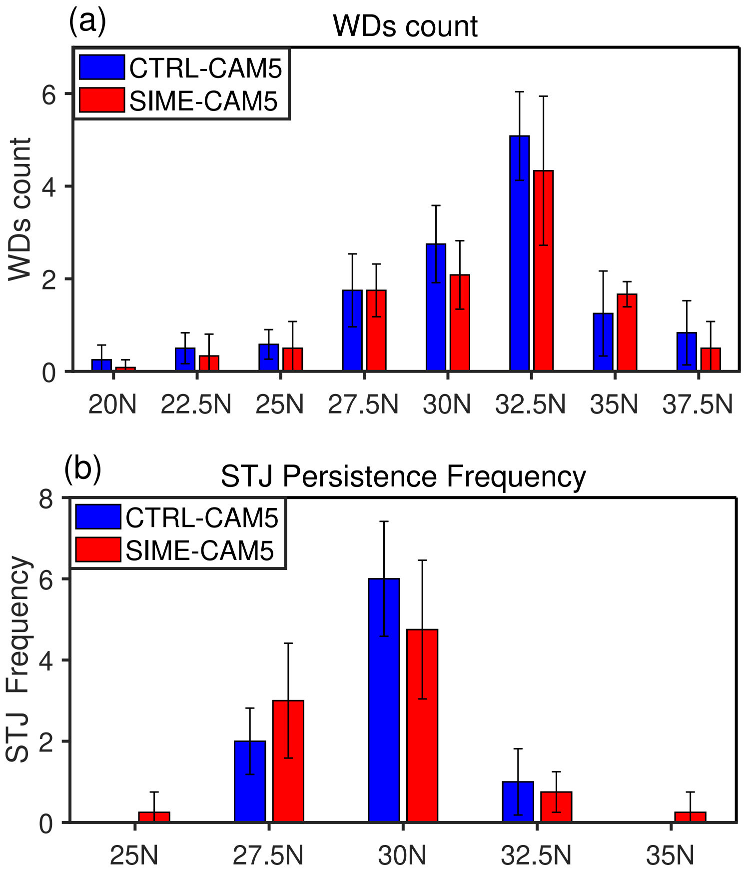


**Fig. 4** Latitudinal distribution of (a) DJF mean WD counts in CTRL-CAM5 and SIME-CAM5 simulations, and (b) The monthly frequency of latitudinal persistence of the subtropical jet for the months of December, January, and February in CTRL-CAM5 and SIME-CAM5 simulations; The latitudinal location of subtropical jet is defined as the latitude of the maximum zonal mean (60°E–85°E) zonal velocity at 200 hPa. The error bars show ensemble spread ($\pm 1$ *std*) of CTRL-CAM5 and SIME-CAM5 runs.

but monthly means for the STJ location. The location of the STJ is more variable and equatorward in SIME-CAM5, being found relatively much more often south of 25°N and slightly more relatively often north of 35°N than in CTRL-CAM5. These regions are unproductive for WD development (Hunt et al., 2018b), contributing to the lower WD frequency seen in SIME-CAM5. Even so, the equatorward spread of the WD distribution in SIME-CAM5 may have consequences for the hydrological cycle since such WDs are much closer to a moisture source (the Arabian Sea) and thus tend to precipitate considerably more (Baudouin et al., 2021).

Recent observational analyses suggest that in recent decades, the lower troposphere over the Arctic has been undergoing an accelerated warming while the upper troposphere and lower stratosphere over the region experiencing a cooling (Serreze and Francis, 2006). This has resulted in a weakening (strengthening) of the equator to pole temperature gradient at lower (upper) tropospheric levels over the northern hemisphere which in turn resulted in an enhanced vertical shear in the extratropical jetstream (Lee et al., 2019). The induced sea ice melt in climate models elicit a similar response in the meridional temperature gradient (Fig. 5). The lower tropospheric DJF mean temperature difference between SIME-CAM5 and CTRL-CAM5 ensembles show a substantial warming poleward of 60°N, in response to the sea ice melt. The pattern of warming in sea ice melt experiments resemble the Arctic amplification (Serreze and Francis, 2006). Equatorward of 60°N, the lower troposphere shows patches of slight cooling over the land region and a weak warming over the oceans, in the SIME-CAM5 runs. Taken together, the stronger warming in the high latitudes and weaker change in the tropics result in an overall weakening of the meridional temperature gradient in the lower troposphere in response to sea ice melt (Fig. 5a). The difference in the DJF mean temperature at 250 hPa between the SIME-CAM5 and CTRL-CAM5 ensembles show a slight cooling over the Arctic region and a strong warming over the subtropics and tropics in response to the sea ice melt, resulting in a strengthening of the upper-tropospheric meridional temperature gradient (Fig. 5b). Also of note is the cooler lower troposphere over Pakistan and North India in SIME-CAM5 compared to CTRL-CAM5. This is very unlikely to be related to the reduced WD activity in SIME-CAM5, since WDs are known to reduce near-surface temperature in this region through enhanced cloud cover, snowfall, and by advection of cool air from higher latitudes (Hunt et al., 2018b; Singh et al., 2019; Sandeep and Prasad, 2020). Instead, this may be related to a continued strengthening of the Karakoram anomaly (Farinotti et al., 2020) or increased cloudburst activity (Kumar et al., 2018).

To explore how these changes might modulate the subtropical jet, we now consider the vertical structure of the meridional temperature gradient. We start by defining the equator-to-pole temperature gradient computed as the difference in the area averaged temperature between two boxes (50°—70°N, 60°—85°E and 20°—36.5°N, 60°—85°E). The DJF mean equator-to-pole temperature gradient at each pressure level in the CTRL-CAM5 simulations show stronger positive values at lower level, with a maximum of about 43 K at 1000 hPa (Fig. 6a). The difference between SIME-CAM5 and CTRL-CAM5 ensembles reveal a weakening of the meridional temperature gradient in the lower to mid-tropospheric levels in the range of -0.5 to -3 K (Fig. 6b). In the upper tropospheric levels, above about 350 hPa, a strengthening of the meridional temperature gradient, with mean values in the range of 0.5 to 3.5 K, can be seen. Lee et al. (2019) attributed a similar pattern of changes observed in the meridional temperature gradient to the Arctic amplification. This contrasting meridional temperature gradients at lower and upper tropospheric levels can result in contrasting thermal wind responses at these levels as suggested by the thermal wind equation:

$$-\frac{\partial u}{\partial p} = -\frac{R}{fp}\frac{\partial T}{\partial y}\,. \tag{1}$$

Fig. 7a shows the difference in the vertical shear of DJF zonal wind between SIME-CAM5 and CTRL-CAM5. The shear in SIME-CAM5 is significantly stronger over the Middle East and northwestern India. The vertical shear of the

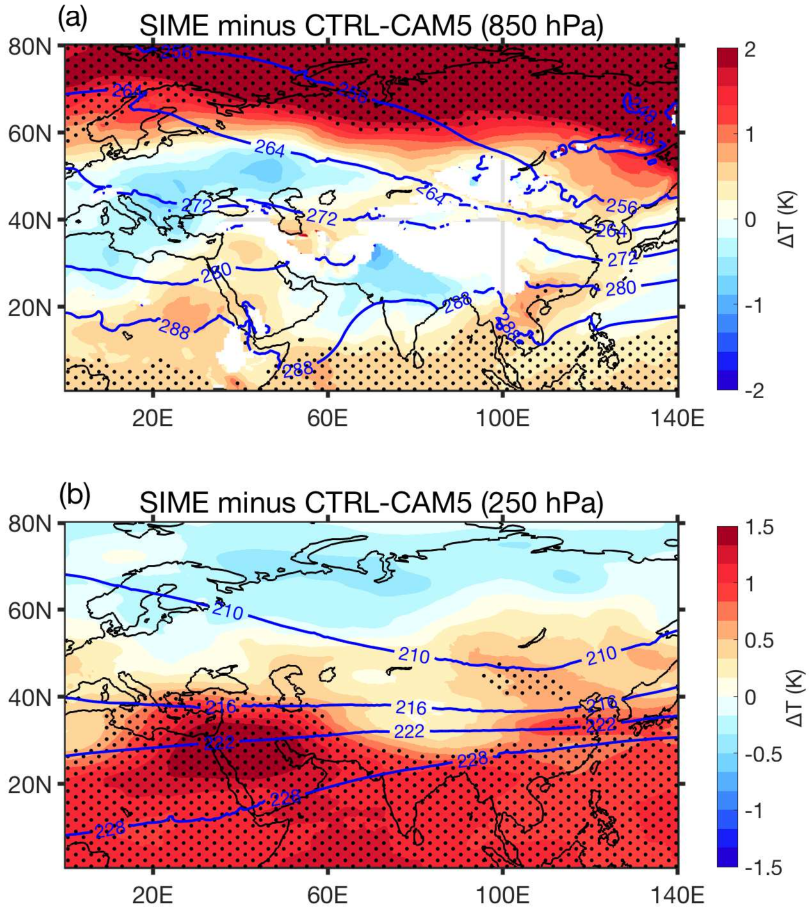


**Fig. 5** DJF mean, ensemble mean temperature difference between SIME-CAM5 and CTRL-CAM5 for (a) 850hPa and (b) 250 hPa. The contours show the CTRL-CAM5 DJF mean temperature at 850hPa and 250 hPa in (a) and (b). Stippling denotes the statistically significant (at 95% confidence level) difference between SIME-CAM5 and CTRL-CAM5, as revealed by a bootstrapping method. Regions in (a) where the climatological 850 hPa level is below the surface are masked.

zonal winds computed from the thermal wind balance shows a close match with that computed directly from the zonal winds (Fig. 7b). This indicates that almost all of the change in the vertical wind shear is caused by the changes in the meridional temperature gradient in the SIME-CAM5 simulations. To show how this imprints on the structure of the jet, we plot a vertical cross-section of DJF zonal wind in Fig. 8, averaged over 60°E-85°E. The two cross-sections show the CTRL-CAM5 ensemble mean (Fig. 8a) and the difference between the SIME-CAM5 and CTRL-CAM5 ensemble means (Fig. 8b). The core of the jet in CAM5-CTRL can be found at about 30°N, consistent with the analysis in Fig. 4a. Although the

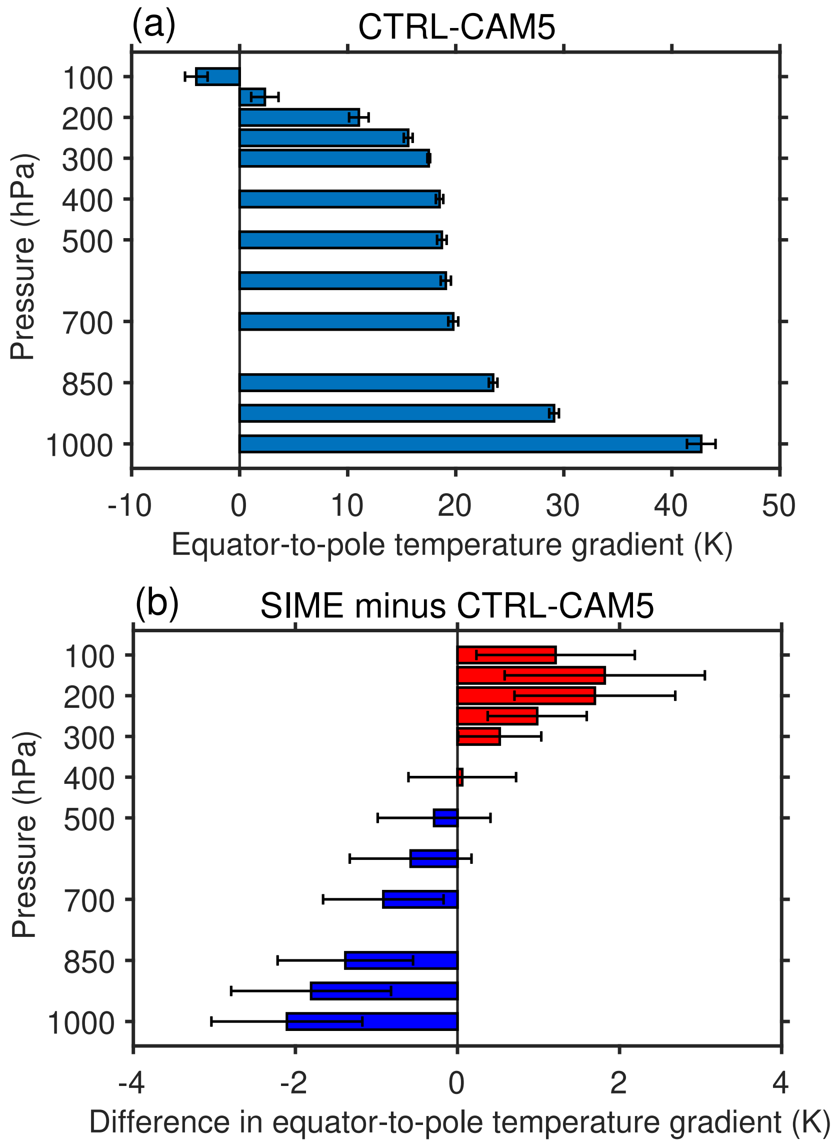


**Fig. 6** DJF mean, ensemble mean of meridional temperature gradient for (a) CTRL-CAM5 and (b) ensemble mean SIME-CAM5 minus CTRL-CAM5 meridional temperature gradient

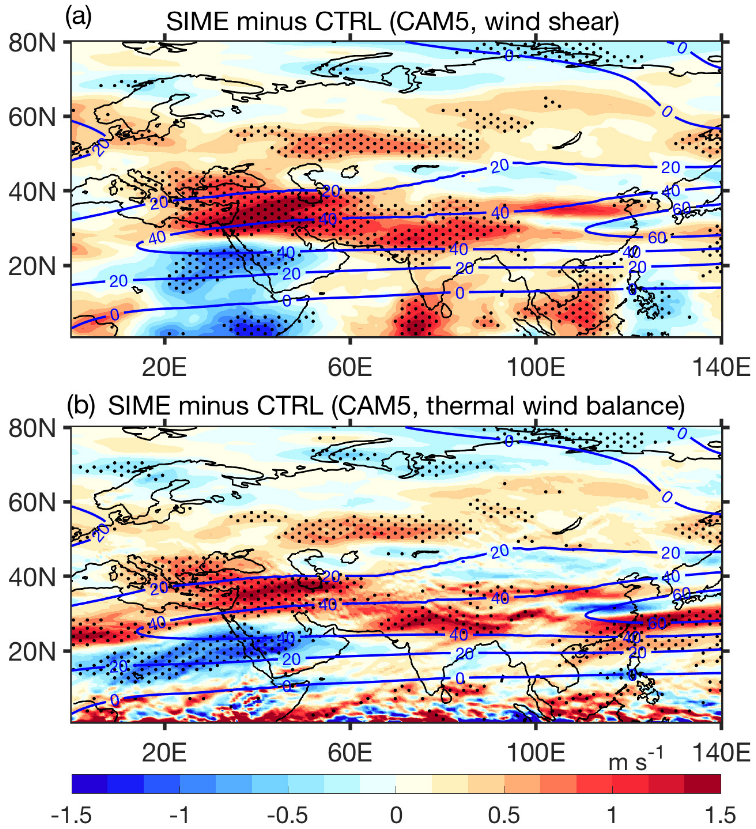


**Fig. 7** DJF mean, ensemble mean difference between SIME-CAM5 and CTRL-CAM5 of vertical shear in zonal wind (U250 - U850), (a) based on actual vertical wind shear calculated from the zonal wind field and (b) the expected vertical wind shear calculated from the temperature field using thermal wind balance. Stippling in (a) and (b) denotes the statistically significant change (at 95% confidence level) , as revealed by a bootstrapping method. Blue contours show the ensemble mean, DJF mean zonal wind at 250 hPa, from CTRL-CAM5.

structure of the subtropical jet in SIME-CAM5 is similar to that in CTRL-CAM5 (Fig. 8b), two significant differences emerge – both driven by the stronger meridional temperature gradient in the upper troposphere. Firstly, the difference pattern shows a significant weakening of the zonal winds poleward of 40°N throughout the tropospheric column. This implies fewer poleward excursions of the subtropical jet during the winter months as it is more firmly locked in place by thermal wind balance (Fig. 7, see also Schiemann et al., 2009). Secondly, there is a signficant widening of the jet – evidenced by stronger westerlies on both its northern (40°N) and southern (15°N) flanks. This persists from the upper-troposphere (200 hPa) into the mid-troposphere (500 hPa), and thus affects WDs, whose vorticity maxima are typically found at around 350 hPa (Hunt et al., 2018b). This widening of the jet makes it more baroclinically stable, and therefore, as we saw in Figs. 2 and 3, it produces less frequent and less intense WDs. This relationship is supported

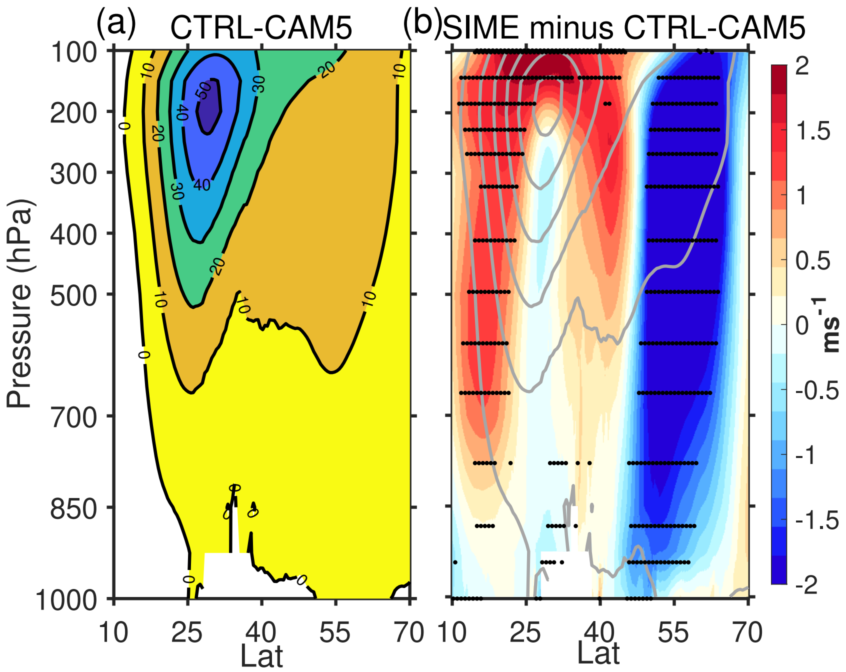


**Fig. 8** DJF mean, ensemble mean zonal wind for (a) CTRL-CAM5 and (b) ensemble mean difference between SIME-CAM5 and CTRL-CAM5 Stippling in (b) denotes the statistically significant change (at 95% confidence level) , as revealed by a bootstrapping method. The contours in (b) show the ensemble mean, DJF mean zonal wind from SIME-CAM5. The cross-section is taken as a zonal average between 60°E and 85°E.

by previous observational studies (Hunt et al., 2018a). Furthermore, the strengthening of each flank of the jet seen in the SIME-CAM5 experiment is asymmetric, with a stronger and more significant increase in zonal winds along the southern flank. This indicates an equatorward shift in the jet in the CAM5-SIME runs, again consistent with the analysis shown in Fig. 4a. Previous observational and modeling studies have also shown that sea ice loss could lead to a weakening, widening, and equatorward shift of the jet (Screen et al., 2013; Peings and Magnusdottir, 2014; England et al., 2018; Screen and Blackport, 2019). The changes in the STJ seen in the SIME-CAM5 ensemble are therefore in line with previous research.

## 4 Conclusions

Although the effect of the Arctic sea ice melt on high and mid-latitude climate was known, the response of low latitude climate has largely been overlooked. Recent investigations, however, suggest that the climate system response to the polar sea ice melt can be detected even in the deep tropics (e.g. Kennel and Yulaeva, 2020). An increasing body of evidence indicates that the large-scale circulation adjustment to the polar sea ice melt includes a weakening, widening, and equatorward shift in mid- and low-latitude jets. This, in turn, raises questions on how the transient weather systems associated with the baroclinicity of these jets might be affected by sea ice melt. However, it is challenging to understand the influence of sea ice melt on such transient weather systems as the coarse resolution of climate models may not resolve important underlying processes. Using a framework of coarse-resolution coupled and high-resolution uncoupled climate model simulations, we examined the response of transient weather systems, known as western disturbances (WDs), which bring substantial winter precipitation to northern India and Pakistan. Our results show that WDs would weaken in both frequency and intensity in response to the polar sea ice melt. We show that this arises as a result of both the widening and an equatorward shift in the subtropical jet, which occurs in response to changes in upper-level meridional temperature gradients. As WDs are important for water security over the western Himalayas and Hindu Kush mountain regions, these results point to serious societal impacts of sea ice melt over places very distant from the high latitudes. The patterns of changes in the jet and the WDs resemble those driven by the greenhouse gas induced warming, suggesting that the feedback of sea ice melt can reinforce the effects of global warming. We argue that further research is needed in understanding the fine scale patterns of low latitude climate response to sea ice melt. A longer (100 y) simulation of coupled model with high-resolution (50 km or less) atmospheric component would be a better framework to study the response of transients to polar sea ice melt, although it would require more computing resources.

## Declarations


- Funding: S. Sandeep is funded by ESSO-National Center for Polar and Ocean Research, Ministry of Earth Sciences (Government of India), under the PACER Outreach Programme (NCPOR/2019/PACER-POP/OS-04). KMRH is funded through the MITRE project, a NERC Independent Research Fellowship (NE/W007924/1).
- Conflict of interest: The authors do not have any conflict of interest
- Ethics approval: Not applicable
- Consent to participate: Not applicable
- Consent for publication: Not applicable
- Availability of data and materials: Data is available from the authors
- Code availability: Codes are available from the authors
- Authors' contributions: SS conceptualised and designed the study; VC performed experiments and data analysis; KMRH tracked WDs; All authors contributed to writing the manuscript.

**Acknowledgements** S. Sandeep acknowledges the financial support by ESSO-National Center for Polar and Ocean Research, Ministry of Earth Sciences (Government of India), under the PACER Outreach Programme (NCPOR/2019/PACER-POP/OS-04), to undertake this research. The model simulations are performed on the high performance computer at IIT Delhi. KMRH is funded through the MITRE project, a NERC Independent Research Fellowship (NE/W007924/1).


## References


Allen RJ, Sherwood SC (2008) Warming maximum in the tropical upper troposphere deduced from thermal winds. Nature Geoscience 1(6):399–403

Baudouin JP, Herzog M, Petrie CA (2021) Synoptic processes of winter precipitation in the Upper Indus Basin. Weather and Climate Dynamics 2(4):1187–1207

Briegleb BP, Light B (2007) A delta-eddington multiple scattering parameterization for solar radiation in the sea ice component of the community climate system model. Tech. Rep. NCAR/TN-472+STR, NCAR

Chandra V, Sandeep S, Suhas E, Subramanian AC (2022) Weakening of indian summer monsoon synoptic activity in response to polar sea ice melt induced by albedo reduction in a climate model. Earth and Space Science DOI 10.1029/2021EA002185

Chevuturi A, Dimri AP (2016) Investigation of Uttarakhand (India) disaster-2013 using weather research and forecasting model. Natural Hazards 82(3):1703–1726

Collins M, Knutti R, Arblaster J, Dufresne JL, Fichefet T, Friedlingstein P, Gao X, Gutowski WJ, Johns T, Krinner G, et al. (2013) Long-term climate change: projections, commitments and irreversibility. In: Climate Change 2013-The Physical Science Basis: Contribution of Working Group I to the Fifth Assessment Report of the Intergovernmental Panel on Climate Change, Cambridge University Press, pp 1029–1136

Comiso JC, Gersten RA, Stock LV, Turner J, Perez GJ, Cho K (2017) Positive trend in the Antarctic sea ice cover and associated changes in surface temperature. Journal of Climate 30(6):2251–2267

Dai H (2021) Roles of surface albedo, surface temperature and carbon dioxide in the seasonal variation of Arctic amplification. Geophysical Research Letters 48(4):e2020GL090301

Deser C, Tomas R, Alexander M, Lawrence D (2010) The seasonal atmospheric response to projected Arctic sea ice loss in the late twenty-first century. Journal of Climate 23(2):333–351, DOI 10.1175/2009JCLI3053.1

Dimri A (2013) Interannual variability of indian winter monsoon over the western himalayas. Global and Planetary Change 106:39–50, DOI https://doi.org/10.1016/j.gloplacha.2013.03.002

Dimri A, Niyogi D, Barros A, Ridley J, Mohanty U, Yasunari T, Sikka D (2015) Western disturbances: a review. Reviews of Geophysics 53(2):225–246

Dimri A, Yasunari T, Kotlia B, Mohanty U, Sikka D (2016) Indian winter monsoon: Present and past. Earth-Science Reviews 163:297–322, DOI https://doi.org/10.1016/j.earscirev.2016.10.008

England M, Polvani L, Sun L (2018) Contrasting the Antarctic and Arctic atmospheric responses to projected sea ice loss in the late twenty-first century. Journal of Climate 31(16):6353 – 6370, DOI 10.1175/JCLI-D-17-0666.1

England M, Polvani L, Sun L, Deser C (2020) Tropical climate responses to projected Arctic and Antarctic sea-ice loss. Nature Geoscience 13:275–281, DOI 10.1038/s41561-020-0546-9

Farinotti D, Immerzeel WW, de Kok RJ, Quincey DJ, Dehecq A (2020) Manifestations and mechanisms of the Karakoram glacier Anomaly. Nature Geoscience 13(1):8–16

Filippi L, Palazzi E, von Hardenberg J, Provenzale A (2014) Multidecadal variations in the relationship between the NAO and winter precipitation in the Hindu Kush–Karakoram. Journal of Climate 27(20):7890 – 7902, DOI 10.1175/JCLI-D-14-00286.1

Francis JA, Vavrus SJ (2012) Evidence linking Arctic amplification to extreme weather in mid-latitudes. Geophysical research letters 39(6)

Francis JA, Vavrus SJ (2015) Evidence for a wavier jet stream in response to rapid Arctic warming. Environmental Research Letters 10(1):014005

Haarsma RJ, Selten F, van Oldenborgh GJ (2013) Anthropogenic changes of the thermal and zonal flow structure over western europe and eastern north atlantic in cmip3 and cmip5 models. Climate dynamics 41(9-10):2577–2588

Harvey BJ, Shaffrey LC, Woollings TJ (2014) Equator-to-pole temperature differences and the extra-tropical storm track responses of the CMIP5 climate models. Climate Dynamics 43(5):1171–1182

Held IM, Hou AY (1980) Nonlinear axially symmetric circulations in a nearly inviscid atmosphere. Journal of Atmospheric Sciences 37(3):515 – 533, DOI 10.1175/1520-0469(1980)037¡0515:NASCIA¿2.0.CO;2

Holland MM, Bitz CM (2003) Polar amplification of climate change in coupled models. Climate Dynamics 21:221–232, DOI 10.1007/s00382-003-0332-6

Houze R, Rasmussen K, Medina S, Brodzik S, Romatschke U (2011) Anomalous atmospheric events leading to the summer 2010 floods in pakistan. Bulletin of the American Meteorological Society 92(3):291–298

Houze R, McMurdie L, Rasmussen K, Kumar A, Chaplin M (2017) Multiscale aspects of the storm producing the june 2013 flooding in uttarakhand, india. Monthly Weather Review 145(11):4447–4466

Hunt KMR, Dimri AP (2021) Synoptic-scale precursors of landslides in the western himalaya and karakoram. Science of The Total Environment 776:145895, DOI https://doi.org/10.1016/j.scitotenv.2021.145895

Hunt KMR, Zaz S (2022) Linking the north atlantic oscillation to winter precipitation over the western himalaya through disturbances of the subtropical jet. Climate Dynamics DOI 10.1007/s00382-022-06450-7

Hunt KMR, Curio J, Turner AG, Schiemann R (2018a) Subtropical westerly jet influence on occurrence of western disturbances and tibetan plateau vortices. Geophysical Research Letters 45(16):8629–8636

Hunt KMR, Turner AG, Shaffrey LC (2018b) The evolution, seasonality and impacts of western disturbances. Quarterly Journal of the Royal Meteorological Society 144(710):278–290

Hunt KMR, Turner AG, Shaffrey LC (2018c) Extreme daily rainfall in pakistan and north india: Scale interactions, mechanisms, and precursors. Monthly Weather Review 146(4):1005–1022

Hunt KMR, Turner AG, Shaffrey LC (2019a) Falling trend of western disturbances in future climate simulations. Journal of Climate 32(16):5037–5051

Hunt KMR, Turner AG, Shaffrey LC (2019b) Representation of western disturbances in CMIP5 models. Journal of Climate 32(7), DOI 10.1175/JCLI-D-18-0420.1

Hunt KMR, Turner AG, Shaffrey LC (2019c) Representation of western disturbances in cmip5 models. Journal of Climate 32(7):1997–2011

Hunt KMR, Turner AG, Schiemann RKH (2021) How interactions between tropical depressions and western disturbances affect heavy precipitation in South Asia. Monthly Weather Review 149(6):1801–1825

Hurrell J, Holland M, Gent P, Ghan S, Kay J, Kushner P, Lamarque J, Large W, Lawrence D, Lindsay K, et al. (2013) The community earth system model: A framework for collaborative research, b. am. meteorol. soc., 94, 1339–1360

Iqbal M, Ilyas K (2013) Influence of icelandic low pressure on winter precipitation variability over northern part of indo-pak region. Arab J Geosci 6:543–548, DOI

10.1007/s12517-011-0355-y

Jahn A, Kay JE, Holland MM, Hall DM (2016) How predictable is the timing of a summer ice-free Arctic? Geophysical Research Letters 43(17):9113–9120

Kennel CF, Yulaeva E (2020) Influence of Arctic sea-ice variability on pacific trade winds. Proceedings of the National Academy of Sciences 117(6):2824–2834, DOI 10.1073/pnas.1717707117

Krishnamurti TN (1961) The subtropical jet stream of winter. Journal of the Atmospheric Sciences 18(2):172–191

Krishnan R, Sabin TP, Madhura RK, Vellore RK, Mujumdar M, Sanjay J, Nayak S, Rajeevan M (2018) Non-monsoonal precipitation response over the Western Himalayas to climate change. Climate Dynamics pp 1–19

Kumar A, Gupta AK, Bhambri R, Verma A, Tiwari SK, Asthana A (2018) Assessment and review of hydrometeorological aspects for cloudburst and flash flood events in the third pole region (Indian Himalaya). Polar Science 18:5–20

Lee SH, Williams PD, Frame TH (2019) Increased shear in the north atlantic upper-level jet stream over the past four decades. Nature 572(7771):639–642

Liu J, Song M, Horton RM, Hu Y (2013) Reducing spread in climate model projections of a september ice-free Arctic. Proceedings of the National Academy of Sciences 110(31):12571–12576

Liu W, Fedorov AV (2019) Global impacts of Arctic sea ice loss mediated by the atlantic meridional overturning circulation. Geophysical Research Letters 46(2):944–952

Mooley D (1957) The role of western disturbances in the production of weather over india during different seasons. MAUSAM 8(3):253–260

NSIDC (2022) National snow and ice data center. DOI https://nsidc.org/cryosphere/snow

Overland JE, Wang M (2013) When will the summer Arctic be nearly sea ice free? Geophysical Research Letters 40(10):2097–2101

Peings Y, Magnusdottir G (2014) Response of the wintertime northern hemisphere atmospheric circulation to current and projected Arctic sea ice decline: A numerical study with cam5. Journal of Climate 27(1):244 – 264, DOI 10.1175/JCLI-D-13-00272.1

Rangachary N, Bandyopadhyay B (1987) An analysis of the synoptic weather pattern associated with extensive avalanching in western himalaya. Int Assoc Hydrol Sci Publ 162:311–316

Ridley J, Wiltshire A, Mathison C (2013) More frequent occurrence of westerly disturbances in Karakoram up to 2100. Science of The Total Environment 468:S31–S35

Sandeep A, Prasad VS (2020) On the variability of cold wave episodes over Northwest India using an NGFS retrospective analysis. Pure and Applied Geophysics 177(2):1157–1166

Sandeep S, Ajayamohan RS, Boos WR, Sabin TP, Praveen V (2018) Decline and poleward shift in indian summer monsoon synoptic activity in a warming climate. Proc Natl Acad Sci USA 115(11):2681–2686, DOI 10.1073/pnas.1709031115

Schiemann R, Lüthi D, Schär C (2009) Seasonality and interannual variability of the westerly jet in the tibetan plateau region. Journal of climate 22(11):2940–2957

Screen JA, Blackport R (2019) How robust is the atmospheric response to projected Arctic sea ice loss across climate models? Geophysical Research Letters 46(20):11406–11415, DOI https://doi.org/10.1029/2019GL084936

Screen JA, Simmonds I (2010) Increasing fall-winter energy loss from the Arctic ocean and its role in Arctic temperature amplification. Geophysical Research Letters 37(16), DOI 10.1029/2010GL044136

Screen JA, Simmonds I, Deser C, Tomas R (2013) The atmospheric response to three decades of observed Arctic sea ice loss. Journal of Climate 26(4):1230 – 1248, DOI 10.1175/JCLI-D-12-00063.1

Screen JA, Deser C, Smith DM, Xiangdong Zhang RB, Kushner PJ, Oudar T, McCusker KE, Sun L (2018) Consistency and discrepancy in the atmospheric response to Arctic sea-ice loss across climate models. Nature Geoscience 11:155–163, DOI 10.1038/s41561-018-0059-y

Serreze M, Francis J (2006) The Arctic amplification debate. Climatic Change 76:241–264, DOI 10.1007/s10584-005-9017-y

Serreze MC, Barry RG (2011) Processes and impacts of Arctic amplification: A research synthesis. Global and Planetary Change 77(1):85 – 96, DOI 10.1016/j.gloplacha.2011.03.004

Singh D, Kumar A, Shekhar MS, Garg S (2019) The impacts of the approaching western disturbances (WDs) on the surface meteorological variables over the north-west Himalaya (NWH), india. Journal of Earth System Science 128(6):1–18

Thompson DW, Solomon S (2005) Recent stratospheric climate trends as evidenced in radiosonde data: Global structure and tropospheric linkages. Journal of Climate 18(22):4785–4795

Yadav RK, Rupa Kumar K, Rajeevan M (2009) Increasing influence of ENSO and decreasing influence of AO/NAO in the recent decades over northwest india winter precipitation. Journal of Geophysical Research: Atmospheres 114(D12), DOI https://doi.org/10.1029/2008JD011318